Asian Journal of Chemistry; Vol. 38, No. 1 (2026), 202-208
ASIAN JOURNAL OF CHEMISTRY
https://doi.org/10.14233/ajchem.2026.35103

Biogenic Synthesis and Characterization of Ag-Zn-CuO Nanoparticles using Peels of *Citrus limetta*: Evaluation of Dyes Degradation and Antibacterial Activity

MADHU KRITI[1], ARPITA ROY[1,*], SARVESH RUSTAGI[2,3], VASEEM RAJA[4] and SWETHA RAJ[5]

[1]Department of Biotechnology, Sharda School of Bioscience & Technology, Sharda University, Greater Noida-201310, India
[2]Department of Food Technology, School of Agriculture, Maya Devi University, Dehradun-248011, India
[3]School of Agriculture Sciences, Shri Guru Ram Rai University, Dehradun-248001, India
[4]Department of Biotechnology, University Centre for Research and Development, Chandigarh University, Gharuan, Mohali-140413, India
[5]Center for Global Health Research, Saveetha Medical College and Hospitals, Saveetha Institute of Medical and Technical Sciences (SIMATS), Chennai-602105, India

*Corresponding author: E-mail: arbt2014@gmail.com

Received: 21 October 2025 *Accepted*: 8 December 2025 *Published online*: 31 December 2025 AJC-22239

The synthesis of green nanomaterials by sustainable routes is gaining more attention as they hold potential for catalysis, environmental clean-up and biomedical applications. Herein, Ag-Zn-CuO trimetallic nanoparticles were green synthesised using *Citrus limetta* (mosambi) peel extract as a bioreducing and stabilizing agent. Phytoconstituents such as phenolics, flavonoids and tannins were present in the peels and help to reduce metal ions and shows capping properties. The formation of nanoparticles was reflected by a clear colour change and further established through UV-Vis spectroscopy, which showed typical SPR absorption bands at 388 nm (Ag), 324 nm (Zn) and 284 nm (CuO). Morphological investigation through FE-SEM reflected uniformly dispersed nanoparticles with irregular surface morphology and EDS ensured their trimetallic nature (84.73 wt.% Ag, 3.06 wt.% Zn, 12.21 wt.% Cu). XRD analysis confirmed crystalline structure by diffraction peaks for fcc Ag (111, 113), Zn (101) and CuO $(\bar{1}13)$ with crystallite size of 16.15 nm on average as calculated from Scherrer's equation. Zeta potential analysis showed a mean value of -16.6 mV and thus moderate electrostatic repulsion to prevent aggregation and promote colloidal stability. Further catalytic application, in the presence of $NaBH_4$, nanoparticles degraded methyl red dye (78.69%) and Congo red dye (73.82%) in 180 min. Antibacterial activity exhibited strong inhibitory activity against *E. coli* (20 mm at 24 mg/mL). Biosynthesised Ag-Zn-CuO trimetallic nanoparticles possess effective dye degradation and antibacterial action, indicating their promise for usage in catalysis, environmental decontamination and biomedical applications.

Keywords: Trimetallic nanoparticles, Mosambi peel, Green synthesis, Congo red, Methyl red, Antibacterial activity.

INTRODUCTION

Nanoparticles have size between 1 and 100 nm in diameter and shows distinct physico-chemical properties from their bulk counterparts. Nanoparticles have high surface area-to-volume ratio, increased chemical activity and significant quantum effects, making them incredibly useful in various areas [1]. Engineered nanoparticles have less weight, stronger mechanical properties, increased durability and more advanced functional attributes. They play a vital role in nanotechnology and their uses have the potential to extend to medicine, electronics, energy and environmental science [2,3]. Different approaches are used to synthesize nanoparticles, of which metal-based nanoparticles are crucial. When they are made up entirely of metallic elements, they are known as metallic nanoparticles [4,5].

The nanoscale sizes of the metal nanoparticles produce special electrical, mechanical and thermal properties that are essentially responsible for their high surface area-to-volume ratio and size-dependent quantum size effects [5-7]. However, even with various benefits, concerns over potential drawbacks have been expressed. Instability in metal nanoparticles may result from their high surface reactivity and their interaction with biological systems can lead to cytotoxicity or organ-based toxicity [8-10]. In addition, their uncontrolled release into the environment could have negatively impact on plants and aquatic ecosystems [11].

To overcome the limitations of monometallic nanoparticles, trimetallic nanoparticles have emerged as promising alternatives, which showed enhances catalytic efficiency and more effective performance. Moreover, the closer electronic and structural integration among different metals imparts greater stability compared to monometallic counterparts, which often have poor durability [12,13]. Strategic metal selection and controlled synthesis further offer opportunities to mitigate toxicity concerns, thereby improving overall biocompatibility and safety. However, synthesis, characterization and biomedical evaluation of trimetallic nanoparticles are still challenging and require large-scale studies to completely describe their mechanistic behaviour, potential hazards and long-term consequences on human and environmental safety [14].

For trimetallic nanoparticle synthesis, various methods like thermal fusion, chemical reduction and microemulsion processes have been reported [15,16]. Of all of these methods, green synthesis is most effective and eco-friendly method. Plant extracts and microbial cultures are used for enabling nanoparticle synthesis, thereby minimizing use of expensive and toxic reagents that are typically used in conventional chemical synthesis [15,17].

Among green synthesis approaches, plant extract mediated methods are generally preferred over microbial-mediated procedures because of their simplicity, scalability and the availability of starting materials. *Citrus limetta* (mosambi) peels, rich in phytochemicals, serve as a green and economically viable precursor for nanoparticle biosynthesis. These peels contain diverse bioactive compounds including flavonoids, phenolics, tannins, saponins, reducing sugars and cardiac glycosides, which act as natural reducing and capping agents, replacing the hazardous chemicals typically used in conventional nanoparticle synthesis [18]. To date, there has been no reported on use of *C. limetta* peels in synthesizing Ag-Zn-CuO trimetallic nanoparticles. The present study used *C. limetta* peel extracts for green synthesis of Ag- Zn-CuO nanoparticles and evaluate its antibacterial and dye degradation activity against selected bacteria and dyes.

EXPERIMENTAL

Dried and ground peels of *Citrus limetta* (mosambi) were utilized as the biological precursor for the trimetallic nanoparticles synthesis. The metal precursors used were silver nitrate ($AgNO_3$), zinc sulphate ($ZnSO_4$) and copper sulphate ($CuSO_4$), all of which were of analytical grade. For assessing catalytic and adsorption efficiency, methyl red (MR) and Congo red (CR) analytical-grade dyes were obtained from SRL Chemicals, Mumbai, India while other reagents required for microbiological assays were purchased from Himedia, India. Bacterial strains used in antimicrobial experiments were obtained from an external collaborating laboratory. Milli-Q water was used to prepare all plant extracts and metal salt solutions to obtain maximum purity and reproducibility of experimental outcomes.

Preparation of *C. limetta* peel extract: *C. limetta* peels were obtained from a nearby juice vendor, it was cleansed thoroughly with milli-Q water to wipe out adherent impurities. The peels were oven-dried at 70 to 80 ºC until they were completely dehydrated and then ground into a fine powder using a sterile mortar and pestle. Powdered material was kept in sterile, airtight polyethylene zipper bags in controlled conditions. For the preparation of extract, 5 g of peel powder was dissolved in 100 mL of milli-Q water and then placed under heating mantle for 15 min. The obtained mixture was left to cool at room temperature and then it was filtered through Whatman grade 1 filter paper to eliminate particulate matter. The filtrate (aqueous peel extract) was collected and stored at 4 ºC for further experiments on nanoparticle synthesis [19].

Synthesis of Ag-Zn-CuO trimetallic NPs: Aqueous 1 mM solutions of $AgNO_3$, $ZnSO_4$ and $CuSO_4$ were prepared in Milli-Q water and stored at 4 ºC in sterile, aseptic containers to prevent degradation or contamination prior to use. Then, Ag-Zn-CuO trimetallic nanoparticles were synthesised by a single-pot simultaneous co-reduction method [20]. *C. limetta* peel extract was initially diluted with 1 mM $AgNO_3$ solution in a 1:9 ratio at room temperature but under continuous stirring, then subjected to 70-80 ºC. An observable change in colour of the reaction mixture confirmed the formation of $AgNO_3$ NPs. Finally, 1 mM $ZnSO_4$ and $CuSO_4$ solutions were sequentially added to the reaction mixture, each followed by an equal volume of peel extract. The mixture was heated for 2 h, changing from bright yellow to black, indicating the formation of Ag-Zn-CuO nanoparticles. After colour stability was observed for 1 h, the colloidal suspension was centrifuged at 10,000 rpm for 5 min, washed twice with Milli-Q water, and re-centrifuged to remove unreacted precursors. The resulting nanoparticles were dried at 70 ºC and stored in sterile containers.

Characterization: UV-Visible spectroscopy was recorded in the wavelength range of 200-800 nm on Thermo-Fisher Scientific Genesys 50 UV-Vis spectrophotometer to track SPR and formation of Ag and ZnO nanoparticles. Field emission scanning electron microscopy (FESEM) coupled with energy dispersive X-ray spectroscopy (EDS) was performed on a ZEISS FESEM instrument to investigate nanoparticle morphology, surface topography and elemental analysis. Identification of the crystal phase and crystal structure was identified *via* X-ray diffraction (XRD) microanalysis on EMPYREAN diffractometer in which diffraction patterns were measured with ranges of 2θ between 20º to 80º confirming the presence of Ag, Zn and CuO phases. Furthermore, the colloidal stability as well as the surface charge of the trimetallic nanoparticles were determined by dynamic light scattering (DLS) and zeta potential measurement by a Litesizer 500 particle size analyzer, reflecting their dispersion properties in different environmental conditions.

Catalytic activity of trimetallic NPs: The catalytic activity of the synthesised Ag-Zn-CuO trimetallic NPs was investigated by reduction of selected organic pollutants *i.e.*, methyl red dye and Congo red dye. The reaction mixtures were prepared by the combination of 1 mg/mL suspension of Ag-Zn-CuO NPs with 15 mM $NaBH_4$ and 1 mM of both dyes (MR and CR). Specifically, 1 mL of stock dye solution was introduced into separate test tubes, followed by 1 mL of $NaBH_4$ solution added sequentially. The next addition was 2 mL of Milli-Q water, making 4 mL as the total volume. Following this, 1 mL of Ag-Zn-CuO NPs suspension was introduced,

providing a final reaction volume of 5 mL. The reaction mixture was incubated in the dark to avoid photodegradation. Catalytic activity was routinely tracked at regular time intervals by UV-Visible spectrophotometry in the range of 200-800 nm. Control experiments, without nanoparticles, were conducted in parallel to deter-mine the inherent effect of $NaBH_4$.

Antibacterial activity: The antibacterial activity of the Ag-Zn-CuO trimetallic nanoparticles synthesised was tested on three clinically significant bacterial strains, *Pseudomonas aeruginosa*, *Escherichia coli* and *Klebsiella pneumoniae* using the conventional agar-well diffusion test. Overnight pre-incubation was given to the bacteria to achieve log-phase growth, followed by uniform spreading over sterile nutrient agar plates to obtain a confluent lawn. Ag-Zn-CuO trimetallic NPs solution (15 mg/mL) was prepared in a 20% DMSO solution and applied to wells on agar plates that were inoculated with nanoparticles in different concentrations (3, 6, 9, 12 mg/mL) for *P. aeruginosa* and *K. pneumoniae*. Further-more, an Ag-Zn-CuO trimetallic NPs solution (30 mg/ mL) was prepared in a 20% DMSO solution for *E. coli* in different concentrations (6, 12, 18, 24 mg/mL). The plates were incubated for 24 h at 37 ºC under aerobic conditions [21].

RESULTS AND DISCUSSION

In present study, a green synthetic synthesis approach was adopted using *Citrus limetta* (mosambi) peel which act as a dual-role stabilizer and bioreductant in the synthesis of Ag-Zn-CuO trimetallic nanoparticles. The peel extract is enriched with diverse phytoconstituents, particularly phenolics, flavonoids and tannins, which possess intrinsic redox potential conducive to metal ion reduction and nanoparticle stabilization. The initial mixture of peel extract with $AgNO_3$ solution exhibited a pale-yellow colouration. Upon sequential incorporation of addition of metal salt precursors under continuous agitation, a distinct colour transformation to dark brown was observed, indicative of nanoparticle nucleation. Subsequent thermal treatment at 70-80 ºC for 1 h yielded a stable black precipitate, confirming the successful formation of Ag-Zn-CuO trimetallic nanoparticles.

UV-Visible studies: The synthesised Ag-Zn-CuO trimetallic NPs were characterized by UV-Visible spectroscopy, which displayed well-defined surface plasmon resonance (SPR) absorption bands at 388 nm, 324 nm and 284 nm, attributable to the characteristic optical responses of Ag, ZnO and CuO NPs, respectively (Fig. 1). Minor spectral shifts are plausibly attributed to the phytochemical-mediated capping interactions from the *C. limetta* peel extract, which modulate nanoparticle size and morphology. These absorption features agree with earlier reports, where AgNPs typically exhibit SPR bands in the range of 360-400 nm due to collective oscillation of conduction band electrons [22], ZnO NPs show the characteristic absorption edges between 355-367 nm associated with their wide band-gap transitions [23] and CuO nanoparticles display absorption bands in the region of 270-300 nm corresponding to the ligand-to-metal charge transfer and band-to-band transitions [24].

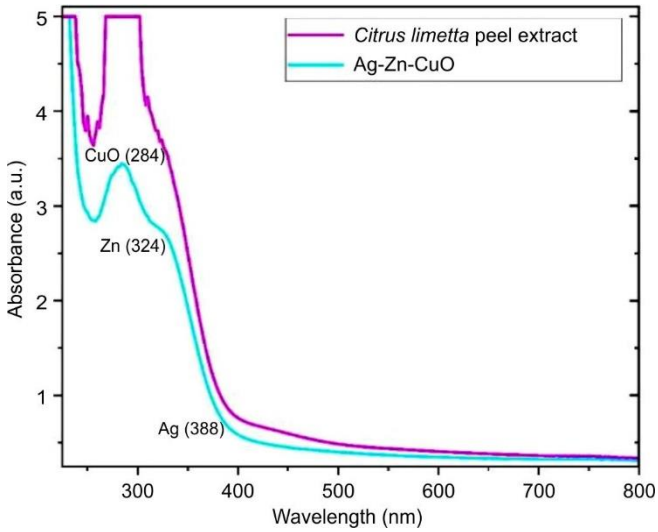

Fig. 1. UV of Ag-Zn-CuO trimetallic nanoparticles

XRD studies: The XRD patterns of synthesised Ag-Zn-CuO trimetallic NPs are shown in Fig. 2. Detail observation of individual XRD patterns and respective diffraction peaks at 2θ confirmed the crystalline character of the synthesised Ag-Zn-CuO trimetallic NPs. The diffraction peaks observed at 38.13º and 77.41º are characteristic of face-centered cubic metallic Ag, corresponding to the (111) and (113) crystallographic planes, respectively, in agreement with the standard JCPDS card no. 04-0783 [25]. In addition, the reflection at 44.31º can be indexed to the (101) plane of Zn, consistent with JCPDS card no. 36-1451 [26]. The peak appears at 64.49º is assigned to the $(\bar{1}13)$ plane of monoclinic CuO, matching well with JCPDS card no. 45-093 [27], thereby confirming the coexistence of Ag, Zn and CuO crystalline phases in the synthesised trimetallic nanoparticles. The average crystal size of Ag-Zn-CuO was calculated as 16.15 nm using Debye-Scherrer's equation:

$$D = \frac{k\lambda}{\beta \cos\theta}$$

where D is the size of the particle size in nm; K is a constant (0.94); λ is the x-ray wavelength (0.154 nm); β is the full width at half maximum (FWHM) of diffracted peaks in radians; and θ is the Bragg angle in radians. Overall, the XRD results confirm the successful formation of crystalline trimetallic NPs with a face-centered cubic structure, demonstrating that Ag, Cu and Zn ions were effectively reduced during the synthesis process. In addition to the well-defined diffraction peaks associated with crystalline phases, the presence of a broad reflection centered around 20º (2θ) indicates the existence of amorphous or poorly ordered regions within the material. Unlike sharp diffraction peaks arising from long-range crystalline order, this broad feature suggests short-range atomic arrangement, which is commonly attributed to nanoscale particle size effects, glassy or weakly crystalline phases or amorphous surface layers coating the crystalline cores, as reported by Monshi *et al.* [28].

FE-SEM and EDS studies: The FE-SEM analysis was carried out using a scale bar of 200 nm, a working distance of 2.8-2.9 mm, accelerating voltage of 5.20 kV and a magnification

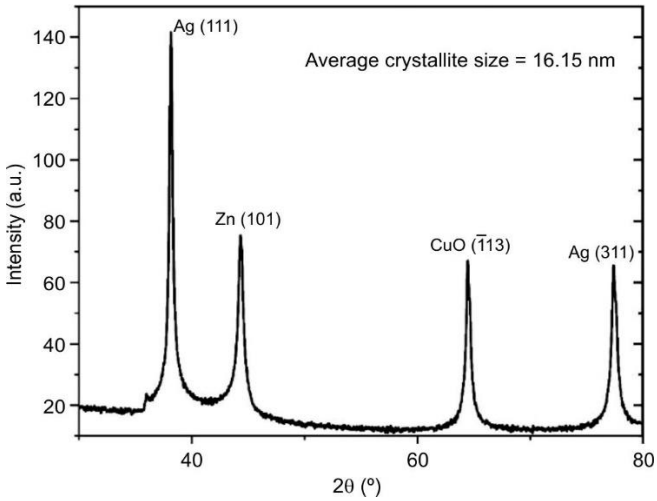

Fig. 2. XRD spectrum of Ag-Zn-CuO trimetallic nanoparticles

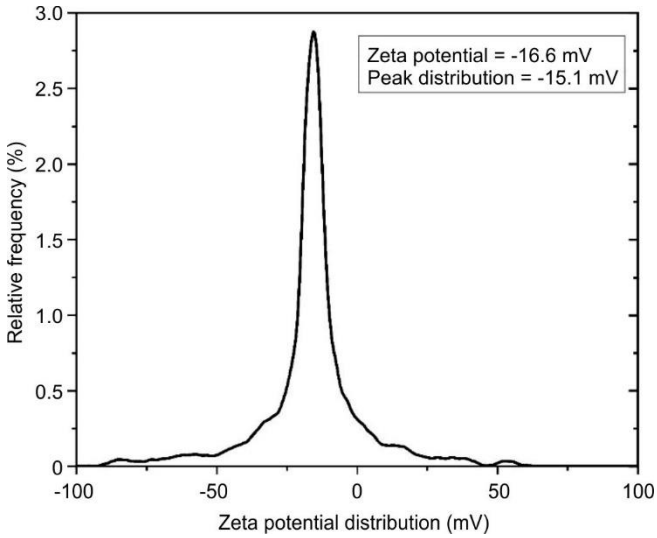

Fig. 4. Zeta potential of Ag-Zn-CuO trimetallic nanoparticles

of 100 KX, which collectively enabled clear visualization of the size distribution and morphological heterogeneity of the trimetallic nanoparticles. The micrograph (Fig. 3a) revealed noticeable surface roughness, a feature of significant importance as it strongly influences surface energy, chemical reactivity and colloidal stability, thereby affecting the overall physico-chemical behaviour and functional performance of the nanoparticles [29]. In addition to the morphological analysis, EDS mapping was utilized to determine the elemental nature of the trimetallic nanoparticles. Quantitative analysis revealed a composition of 87.79 wt.% Ag, 0 wt.% Zn and 12.21 wt.% Cu.

Zeta potential: Variations in zeta potential play a critical role in nanoparticle stability, as higher absolute values (either positive or negative) generate stronger electrostatic repulsive forces that inhibit particle aggregation, while lower absolute values diminish this repulsion, thereby promoting flocculation and phase separation under destabilizing conditions. In this study, zeta potential measurements were performed using the Litesizer 500 instrument. The zeta potential of Ag-Zn-CuO trimetallic nanoparticles was found to exhibit a mean value of -16.6 mV, with a peak distribution at -15.1 mV and a standard deviation of 0 mV (Fig. 4), indicating a uniform charge distribution. The surface charge and colloidal stability of the trimetallic nanoparticles are governed by their atomic composition and morphological features. Monometallic Ag nanoparticles exhibit a zeta potential of approximately -19.7 mV, while monometallic Zn nanoparticles show relatively higher absolute zeta potential values of around ±35 mV, reflecting enhanced electrostatic stability [30]. In contrast, monometallic CuO nanoparticles reported to possess a comparatively lower zeta potential of about -11.7 mV, indicating reduced colloidal stability [31].

The mean zeta potential of -16.6 mV indicates the presence of a moderately negative surface charge, which provides sufficient electrostatic repulsion to partially counteract particle aggregation and thereby support colloidal stability. In addition, the peak observed at -15.1 mV suggests a fraction of nanoparticles with a relatively higher density of negative surface charge, contributing further to the overall stability of the dispersion. Such electrostatic stability is particularly important for practical applications, as it enables Ag-Zn-CuO trimetallic nanoparticles to retain dispersion integrity during use in heterogeneous catalysis, biosensing systems, and

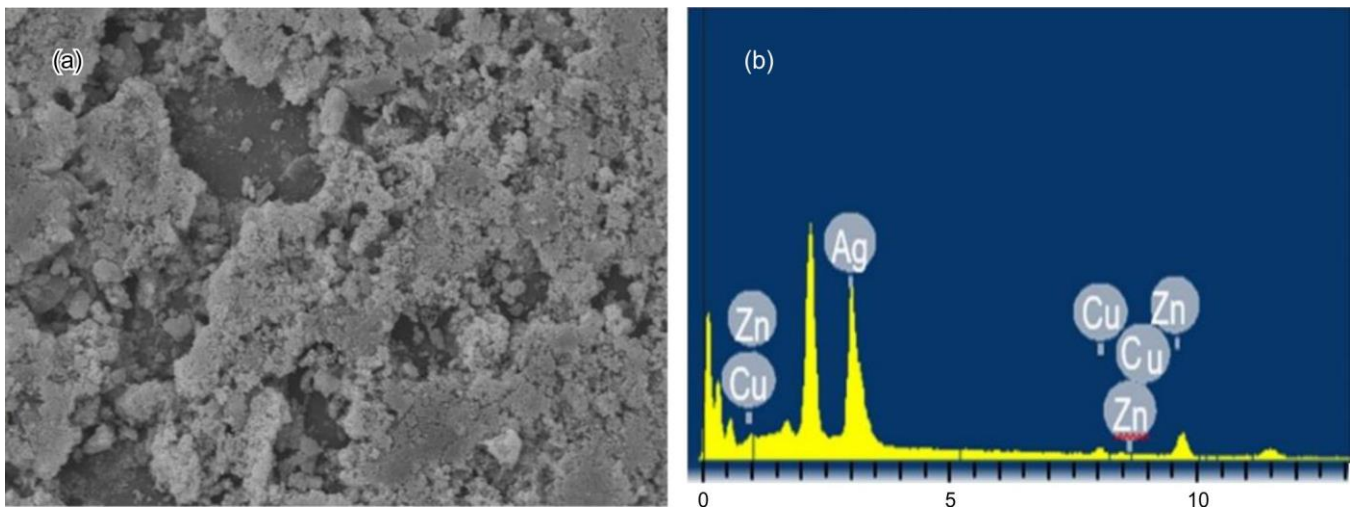

Fig. 3. (a) FE-SEM and (b) EDS analysis of Ag-Zn-CuO trimetallic nanoparticles

biomedical applications, minimizing undesired aggregation or sedimentation [32].

Antibacterial activity: The antibacterial activity of the biogenic Ag-Zn-CuO trimetallic nanoparticles was evaluated against *P. aeruginosa*, *K. pneumoniae* and *E. coli*. The well diffusion technique was employed to evaluate the antibacterial activity [33]. Varying concentrations of Ag-Zn-CuO nanoparticles were employed for antibacterial treatments, with doses of 3, 6, 9, and 12 mg/mL applied against *P. aeruginosa* and *K. pneumoniae*, while higher concentrations of 6, 12, 18, and 24 mg/mL were used for *E. coli*. All the bacterial strains were inhibited by a diffused ring formed by the aqueous solution of the Ag-Zn-CuO trimetallic nanoparticles ranging from 0 mm to 25 mm. The Ag-Zn-CuO trimetallic nanoparticles exhibit satisfactory inhibitory action against *K. pneumoniae* (12 mm), *P. aeruginosa* (11 mm) at 12 mg/mL. Moreover, higher inhibitory activity was shown against *E. coli* (20 mm) at 24 mg/mL (Fig. 5). However, based on results, the synthesised trimetallic nanoparticles exhibited stronger inhibitory activity against *E. coli* and *K. pneumoniae* compared to the positive control. Although the antibacterial effect against *P. aeruginosa* was comparatively lower, a clear and statistically significant level of inhibition was still observed.

Dye degradation efficiency: Since, sodium borohydride ($NaBH_4$) alone showed negligible dye degradation, as confirmed by control experiments, indicating its intrinsically slow reaction rate. In contrast, the presence of Ag-Zn-CuO trimetallic nanoparticles markedly enhanced the catalytic efficiency of the $NaBH_4$ system, owing to their high specific surface area and surface reactivity, resulting in an increased reaction rate constant and confirming their effective nanocatalytic role [34]. Using this catalytic system, methyl red degradation reached 78.69% within 180 min, while Congo red was reduced by 73.82% (Fig. 6).

Conclusion

The Ag-Zn-CuO trimetallic nanoparticles were successfully synthesized through a green route using *Citrus limetta* peel extract, demonstrating a sustainable, cost-effective and environmentally benign approach to nanoparticles fabrication. The phytochemical constituents of the peel extract functioned simultaneously as reducing and stabilizing agents, eliminating the need for hazardous chemicals and energy-intensive synthesis routes. The resulting trimetallic nanoparticles exhibited superior functional performance, showing notable antibacterial activity and high catalytic efficiency, with degradation efficiencies of 78.69%

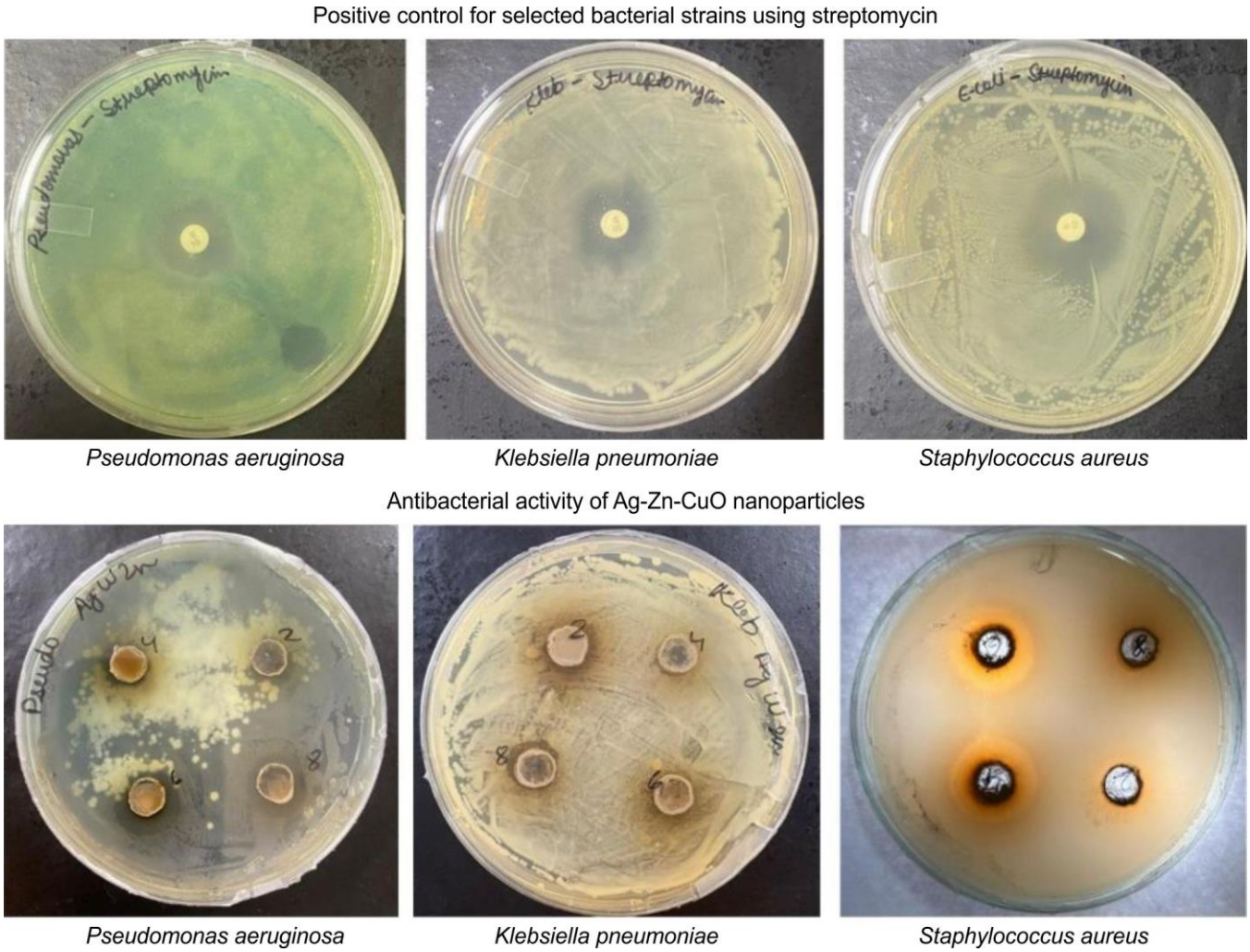

Fig. 5. Antibacterial of Ag-Zn-CuO trimetallic nanoparticles and positive control (streptomycin) against selected bacteria

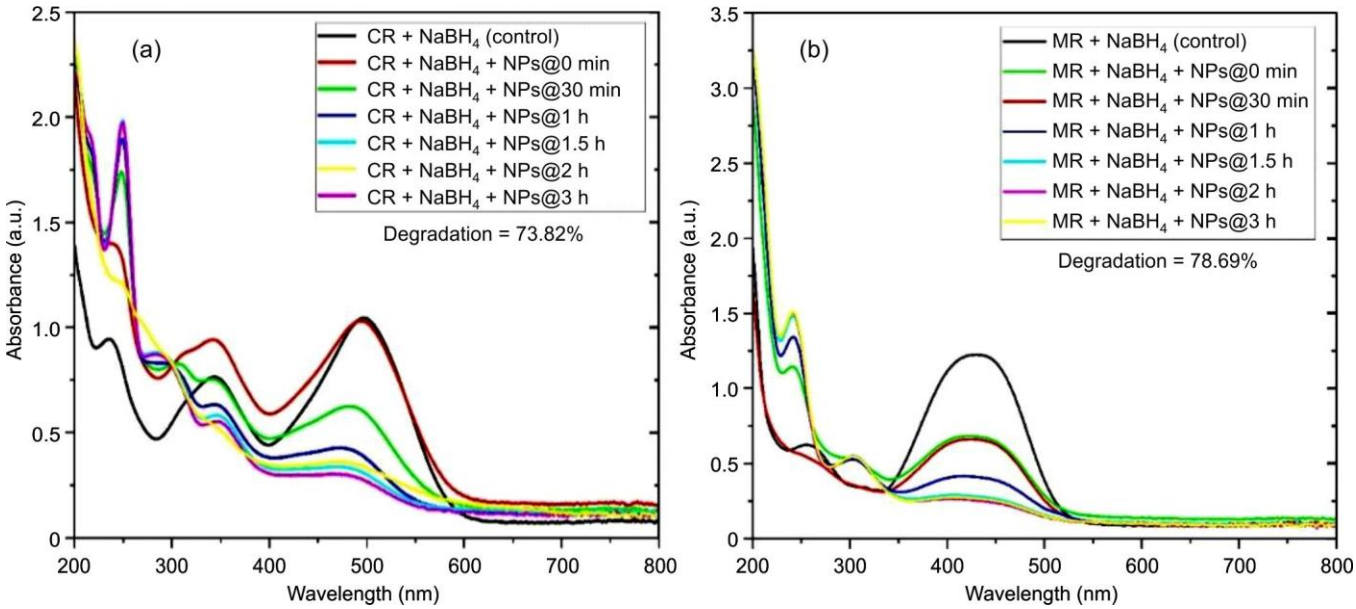

Fig. 6. Degradation of Congo red (CR) and methyl red (MR) using Ag-Zn-CuO trimetallic nanoparticles

for methyl red and 73.82% for Congo red within 18s0 min. The enhanced catalytic and antimicrobial properties are attributed to the synergistic effects arising from the trimetallic composition. Overall, this study validates fruit peel mediated green synthesis as an effective strategy for producing multifunctional nanomaterials with potential applications in environmental remediation and antimicrobial systems.

ACKNOWLEDGEMENTS

The authors thank their respective institutions for providing the constant support and research facilities.

CONFLICT OF INTEREST

The authors declare that there is no conflict of interests regarding the publication of this article.

DECLARATION OF AI-ASSISTED TECHNOLOGIES

During the preparation of this manuscript, the authors used an AI-assisted tool(s) to improve the language. The authors reviewed and edited the content and take full responsibility for the published work.

REFERENCES

1. Z. Zulfiqar, R.R.M. Khan, M. Summer, Z. Saeed, M. Pervaiz, S. Rasheed, B. Shehzad, F. Kabir and S. Ishaq, *Biocatal. Agric. Biotechnol.*, **57**, 103121 (2024); https://doi.org/10.1016/j.bcab.2024.103121
2. A. Bieliatynskyi, L. Bouziane, O. Bakulich, V. Trachevskyi and M. Ta, *Rev. Chem. Eng.*, (2025); https://doi.org/10.1515/revce-2025-0037
3. V. Harish, D. Tewari, M. Gaur, A.B. Yadav, S. Swaroop, M. Bechelany and A. Barhoum, *Nanomaterials*, **12**, 457 (2022); https://doi.org/10.3390/nano12030457
4. A.I. Osman, Y. Zhang, M. Farghali, A.K. Rashwan, A.S. Eltaweil, E.M. Abd El-Monaem, I.M.A. Mohamed, M.M. Badr, I. Ihara, D.W. Rooney and P.-S. Yap, *Environ. Chem. Lett.*, **22**, 841 (2024); https://doi.org/10.1007/s10311-023-01682-3
5. M. Shahalaei, A. K. Azad, W. M. A. W. Sulaiman, A. Derakhshani, E. B. Mofakham, M. Mallandrich, V. Kumarasamy and V. Subramaniyan, *Front. Chem.*, **12**, 1398979 (2024); https://doi.org/10.3389/fchem.2024.1398979
6. C.N.R. Rao, G.U. Kulkarni, P.J. Thomas and P.P. Edwards, *Chem. Soc. Rev.*, **29**, 27 (2000); https://doi.org/10.1039/A904518J
7. J.-T. Lue, *J. Phys. Chem. Solids*, **62**, 1599 (2001); https://doi.org/10.1016/S0022-3697(01)00099-3
8. P. Akhtar, A. B. Haque, and S. Khan, *Toxicol. Lett.*, **355**, 62 (2021); https://doi.org/10.1016/j.toxlet.2021.06.009
9. S. Sharma, N. Sharma, and R.K. Sharma, *Nanomaterials*, **12**, 1234 (2022); https://doi.org/10.3390/nano12081234
10. M. Nel, L. Xia, G. Mädler and N. Li, *Science*, **311**, 622 (2006); https://doi.org/10.1126/science.1114397
11. V. Chandrakala, V. Aruna and G. Angajala, *Emergent Mater.*, **5**, 1593 (2022); https://doi.org/10.1007/s42247-021-00335-x
12. R. Rajeev, A. Varghese, M. Kaur, S. Garg and A. Nakai, *Nanoscale Adv.*, (2025); https://doi.org/10.1039/D5NA00936G
13. J.W.M. Crawley, I.E. Gow, N. Lawes, I. Kowalec, L. Kabalan, C.R.A. Catlow, A.J. Logsdail, S.H. Taylor, N.F. Dummer and G.J. Hutchings, *Chem. Rev.*, **122**, 6795 (2022); https://doi.org/10.1021/acs.chemrev.1c00493
14. A.H. Hashem, E. Saied, B.M. Badr, M.S. Dora, A.M. Abdelaziz, M.A. Diab, F.M. Elkady, M.A. Ali, N.I. Issa, Z.A. Hamdy, M.E. Nafea, A.N. Khalifa, A. Adel, A. Hasib, A.M. Hawela, M.M. El-Gazzar, M.A. Nouh, A.A. Nahool and M.S. Attia, *Arch. Microbiol.*, **207**, 50 (2025); https://doi.org/10.1007/s00203-025-04237-y
15. M. Nasrollahzadeh, M. Sajjadi, S. Iravani and R.S. Varma, *Nanomaterials*, **10**, 1784 (2020); https://doi.org/10.3390/nano10091784
16. Y. Chen, A. Zohaib, H. Sun and S. Sun, *Chem. Commun.*, **61**, 12097 (2025); https://doi.org/10.1039/D5CC01468A
17. T.S. Merjan and Z.T.A. Ali, *Desalination Water Treat.*, **322**, 101082 (2025); https://doi.org/10.1016/j.dwt.2025.101082
18. M.U. Rashid, S.J. Shah, S. Attacha, L. Khan, J. Saeed, S.T. Shah and H.I. Mohamed, *Waste Biomass Valoriz.*, **15**, 3351 (2024); https://doi.org/10.1007/s12649-023-02389-w
19. S. Suri, A. Singh, P.K. Nema, S. Malakar and V.K. Arora, *Food Biosci.*, **48**, 101789 (2022); https://doi.org/10.1016/j.fbio.2022.101789
20. M.H. Salmani, M. Abedi, S.A. Mozaffari, A.H. Mahvi, A. Sheibani and M. Jalili, *J. Environ. Health Sci. Eng.*, **19**, 603 (2021); https://doi.org/10.1007/s40201-021-00631-y

21. A. Menichetti, A. Mavridi-Printezi, D. Mordini and M. Montalti, *J. Funct. Biomater.*, **14**, 244 (2023); https://doi.org/10.3390/jfb14050244
22. A. Marukurti, A.M. Reddy, P.V. Nirmala, D. Kalyani, K. Ramaneswari, I.J.N. Padmavathi, L.P. Pemmaraju, G.S. Silvanus, B.S. Keerthana, S. Farhana, D. Ramachandran, B. Mallikarjuna and P.B. Kasi, *Sci. Rep.*, **15**, 28303 (2025); https://doi.org/10.1038/s41598-025-14353-w
23. A.N. Abdulqodus, A.F. Abdulrahman, S.H. Mostafa, A.A. Kareem, S.M. Hamad, S.M. Ahmed, M.A. Almessiere and D. Shaikhah, *Appl. Phys. A*, **131**, 720 (2025); https://doi.org/10.1007/s00339-025-08874-4
24. P. Mallick and S. Sahu, *Nanosci. Nanotechnol.*, **2**, 71 (2012); https://doi.org/10.5923/j.nn.20120203.05
25. N.P.U. Nguyen, N.T. Dang, L. Doan and T.T.H. Nguyen, *Processes*, **11**, 2617 (2023); https://doi.org/10.3390/pr11092617
26. E. Ramya, M.V. Rao, L. Jyothi and D.N. Rao, *J. Nanosci. Nanotechnol.*, **18**, 7072 (2018); https://doi.org/10.1166/jnn.2018.15521
27. T. Chutimasakul, P. Na Nakhonpanom, W. Tirdtrakool, A. Intanin, T. Bunchuay, R. Chantiwas and J. Tantirungrotechai, *RSC Adv.*, **10**, 21009 (2020); https://doi.org/10.1039/D0RA03884A
28. A. Monshi, M.R. Foroughi and M.R. Monshi, *World J. NanoSci. Eng.*, **2**, 154 (2012); https://doi.org/10.4236/wjnse.2012.23020
29. A. Król-Górniak, V. Railean, P. Pomastowski, T. Płociński, M. Gloc, R. Dobrucka, K.J. Kurzydłowski and B. Buszewski, *Sci. Rep.*, **13**, 587 (2023); https://doi.org/10.1038/s41598-023-27564-w
30. U. Kamran, H.N. Bhatti, M. Iqbal, S. Jamil and M. Zahid, *J. Mol. Struct.*, **1179**, 532 (2019); https://doi.org/10.1016/j.molstruc.2018.11.006
31. M.A. Ahmad, R. Javed, M. Adeel, M. Rizwan, Q. Ao and Y. Yang, *Molecules*, **25**, 1356 (2020); https://doi.org/10.3390/molecules25061356
32. A.H. Shah and M.A. Rather, *Mater. Today Proc.*, **44**, 482 (2021); https://doi.org/10.1016/j.matpr.2020.10.199
33. M. Alavi, E. Jabari and E. Jabbari, *Expert Rev. Anti-Infect. Ther.*, **19**, 35 (2021); https://doi.org/10.1080/14787210.2020.1810569
34. Y. Wu, R.N. Elhouda Tiri, M. Bekmezci, E.E. Altuner, A. Aygun, C. Mei, Y. Yuan, C. Xia, E.-N. Dragoi and F. Sen, *Int. J. Hydrogen Energy*, **48**, 21055 (2023); https://doi.org/10.1016/j.ijhydene.2022.07.152